Environmentally Friendly Interferometry

Leslie L. Deck*
Zygo Corporation
Laurel Brook Road, Middlefield, CT. 06455-0448

ABSTRACT

Combining spatial and time-domain processing in wave-front measuring interferometers is a powerful tool for reducing the influence of environmental disturbances on the measurement. Modern digital imagers and computing platforms eliminate most of the disadvantages typically cited against spatial processing techniques. The ability to perform both spatial and time-domain processing in a single instrument provides the greatest flexibility for precision metrology applications in both static and dynamic environments.

Keywords: Interferometry, phase shifting, metrology, carrier fringe, vibration, turbulence.

1. INTRODUCTION

Phase Shifting Interferometry [1] (PSI) has been the preferred measurement technique for high-precision wave-front measurements for over 30 years. The technique utilizes an electronic imaging system to store a sequence of interferograms with well-known cavity phase-shifts and a computer recovers the original wave-front phase by an analysis of the variation of intensity as a function of phase-shift. Unfortunately, PSI can perform poorly in the presence of environmental disturbances such as acoustical or mechanical vibrations or air turbulence. The main reason for the environmental sensitivity is that the measurement sequence takes time, so cavity optical path variations due to changing environmental conditions during the measurement alter the expected phase variation and produce errors in the wave-front determination.

Different schemes to minimize environmental influences in PSI have been proposed and fit broadly into three categories; least-squares processing, time domain processing and space domain processing.

Least-squares processing, described by Greivenkamp [2], Okada et. al.[3] and later by Kim et. al.[4, 5], attempt to use the fact that an acquisition of four or more phase-shifted interferograms provides, in principle, enough information to calculate the wave-front while treating the cavity phase increments as unknowns. In order to over determine the problem and make it amenable to a solution, the Authors often restrict the spatial dependence of the phase shifts, which may be unrealistic in the presence of turbulence. Furthermore, iterative nonlinear methods are used to find the solutions, and they do not always converge to the optimum solution quickly or deterministically, especially since significant cross-dependencies exist between the variables.

Time domain processing methods generally acquire multiple phase-shifted interferograms significantly faster than the expected vibrational bandwidth in order to minimize environmentally induced cavity motion. Examples include quadrature methods[6, 7], multi-sensor methods[8], and instantaneous phase-shift methods[9, 10]. Each of these methods have disadvantages in the form of requiring either additional hardware, specialized or multiple imagers, reduced system light efficiency, or are incompatible with Fizeau interferometer geometries.

Spatial domain processing (Fourier transform method) was first described by Takeda et al.[11] for 1-dimensional interferograms and was subsequently extended to 2-D by Macy[12]. A review of the technique can be found in Malacara [13]. The technique involves introducing tilt fringes into the interferogram as a carrier for the cavity optical path variation. The wave-front phase is recovered by identifying and isolating the carrier frequency with a digital filter in the spatial frequency domain and inverse transforming the filtered spectrum. Since only a single interferogram is required, vibrational motion is "frozen" and does not influence the wave-front determination. Turbulence on the other hand, being

* email: ldeck@zygo.com

stochastic in nature and having typically a higher spatial variation than vibration, can be effectively handled by averaging a large number of measurements. The Zeiss Direct 100[14] is probably the best example of a precision interferometer using spatial processing techniques. The main disadvantages of this method are generally regarded to be reduced spatial resolution and dynamic range, and the introduction of wave-front aberrations due to the tilted geometry. The former disadvantage was addressed by Kuechel and Hof[15], who were the first to consider combining both spatial and temporal processing in the context of projection Moire to obtain the best features of both processing methods, with Goldberg and Bokor extending this idea to PSI[16]. The latter disadvantage can be handled with aberration subtraction techniques.

In this paper I reconsider spatial domain processing techniques in light of the capabilities of modern imagers and computers, and show that the reasons underlying most preconceived disadvantages are either no longer applicable or are no worse than competing techniques. The conclusion is that a conventional Fizeau interferometer with both PSI and spatial phase processing capability is a versatile tool for performing precision metrology in both static and dynamic environments.

2. CARRIER FRINGE INTERFEROMETRY

Following typical derivations of the Fourier-transform analysis method, the intensity distribution of the spatial interferogram with tilt fringes can be written as

$$p(\vec{r}) = a(\vec{r}) + b(\vec{r})\cos\left(q(\vec{r}) + \vec{k}_0 \cdot \vec{r}\right) = a(\vec{r}) + d(\vec{r})\exp\left(i\vec{k}_0 \cdot \vec{r}\right) + d^*(\vec{r})\exp\left(-i\vec{k}_0 \cdot \vec{r}\right), \quad (1)$$

where $q(\vec{r})$ is the phase variation to be solved for, $\vec{k}_0$ is the carrier frequency, $\vec{r}$ is the spatial coordinate vector and

$$d(\vec{r}) = b(\vec{r})\exp\left(iq(\vec{r})\right)/2. \quad (2)$$

The Fourier transform of this expression leads to

$$FT\left[p(\vec{r})\right] = P(\vec{k}) = A(\vec{k}) + D(\vec{k} - \vec{k}_0) + D^*(\vec{k} + \vec{k}_0), \quad (3)$$

with $A(k)$ and $D(k)$ being the Fourier transforms of $a(r)$ and $d(r)$ respectively. The three terms in Eq. (3) represent the DC and the positive and negative frequencies of the carrier signal modulated by the cavity phase distribution. The idea is to isolate one of the $D(k)$ terms with a digital filter and inverse Fourier transform to produce a complex surface map $C(r)$,

$$C(\vec{r}) = FT^{-1}\left[Filter\left[FT\left[p(\vec{r})\right]\right]\right]. \quad (4)$$

A tilted replica of the phase distribution is extracted from the complex surface map with

$$f(\vec{r}) = \arg\left[C(\vec{r})\right] = \tan^{-1}\left[\mathrm{Im}\left(C(\vec{r})\right)/\mathrm{Re}\left(C(\vec{r})\right)\right]. \quad (5)$$

As with PSI, the principle value of the arctan function produces a phase distribution modulo 2π, which must be unwrapped (and detrended) to obtain the wave-front phase distribution.

Which $D(k)$ in Eq. (3) is isolated by the filter will affect the sign of the extracted phase distribution, reflecting the inherent ambiguity in the fringe direction. This is a minor inconvenience which is easily handled by knowing the sign of the tilt. The noteworthy feature is that the surface phase distribution is obtained with a single spatial interferogram, "freezing out" any vibrational motion, and turbulence affects can be reduced by simple averaging.

The question therefore is, what are the disadvantages of such a simple analysis technique and how does it compare with competing techniques in environmentally dynamic situations. It turns out that many of the perceived disadvantages are vestiges of historical problems which were manifest when the technique was first explored, while others can be overcome using the computing power available today. Still others are just as common in competing techniques. The following is a discussion of the various issues.

Spatial intensity variation: A fundamental restriction of the Fourier transform method that the spectral content of the test surface reflectivity (or the illumination intensity) be outside the bandwidth of the isolation filter so that spectral overlap is minimized. This is typically not a practical limitation for large aperture applications, however the combined spatial and temporal processing technique discussed in Section 4 minimizes this restriction without increasing environmental sensitivity.

Improvements in Detectors: The carrier fringe technique can be influenced by spatial imperfections in the detector, such as fixed pattern noise, unstable black levels and image distortion. This was of great concern early on when detectors such as vidicon cameras were employed. The capability of current digital camera technology makes these issues almost insignificant. Large format imagers with superb uniformity, low fixed pattern noise and lithographically precise sampling are now common.

Spatial resolution and departure dynamic range: The spatial resolution of the carrier fringe technique depends primarily on the imager sampling density and the characteristics of the frequency domain filter. The highest resolution attainable is ½ Nyquist since at least ½ of the frequency domain information is discarded by the filter. I discuss later a particular filter which maximizes the lateral resolution. As expected, this restriction also limits the maximum allowable local surface departure to one that produces a fringe density of ½ Nyquist. Instantaneous phase techniques that use a single imager all have similar limits; multiple (or larger format) imagers are required to exceed it. Resolution to Nyquist can be recovered in a dynamic environment with a combined spatial and temporal processing technique as discussed in Section 4.

Non-common path geometry: The tilted optical geometry means that the returning test and reference wave-fronts are not completely common path, increasing influences associated with optical fabrication errors since the returning wave-fronts probe different regions of the optic. However competing instantaneous phase techniques require that the test and reference wave-fronts are separable, either via polarization or by spatially separating them at the system focus. Polarization separation is incompatible with a Fizeau geometry, necessitating fundamentally non-common path optical geometries like Michelson or Twyman-Green with associated greater sensitivity to optical fabrication errors and environmental differences between the two paths. A Fizeau geometry with separated wave-fronts at the system focus is optically equivalent to the carrier fringe technique, with identical non-common path issues.

Off-axis propagation aberrations: Coma and astigmatism are the dominant aberrations produced in a tilted geometry which for high precision applications must be removed. One method is to calculate the aberrations for the particular optical system used with a commercial ray-trace program at a particular tilt, express them as Zernike coefficients and scale the coefficients according to the functional dependence on tilt magnitude and direction. For example, coma scales with the tilt magnitude whereas astigmatism scales with the square of the tilt magnitude. The aberration map, once appropriately scaled for the measured tilt, is subtracted from the measurement to remove the tilt induced aberrations. As was shown by Evans[17], this can be done with a high degree of accuracy. An alternative is to create an aberration map via the difference between a tilted and untilted PSI measurement, and subtract this aberration map from subsequent carrier fringe measurements performed at the same tilt. This self-calibration method is a compelling motivation for providing both PSI and carrier fringe measurement capability in the same instrument. We have found these correction methods provide better than $\lambda/50$ accuracy for spherical measurements across the optical configurations available in our commercial instruments.

Improved processing power: Performing the required forward and inverse 2-dimensional Fourier transforms on large format images taxed even the most advanced computers when the carrier fringe technique was first introduced over 30 years ago. However, megapixel images can be processed in less than a second with the personal computers manufactured today.

Ease of use: The main ease of use issue in carrier fringe techniques is tilt ambiguity. As stated earlier, with only a single interferogram, the analysis requires an additional piece of information to determine the sign of the tilt. This additionally information can be user supplied, determined by restricting the available tilt options or by measurement; for example dynamically by analyzing another interferogram after imparting a known phase shift, or statically by imaging the Fourier plane directly.

Edge artifacts: The Fourier series representation of a discontinuous function contains ringing in an effect called the Gibbs phenomenon. The effect can produce distortion near boundaries between fringe regions and fringeless regions. The ringing is reduced as the sampling density increases and under most situations in large aperture interferometry,

discarding a few pixels near boundaries is an effective method for removing these artifacts. For those cases where this cannot be done, the ringing can be substantially reduced by setting the fringeless regions to the DC intensity or by analytically continuing the fringed region into the fringeless region.[18] Additionally, as will be discussed below, edge artifacts can be eliminated by averaging a number of phase-shifted frames, or with a combined spatial and temporal processing technique like that proposed by Goldberg[16].

3. ENVIRONMENTALLY FRIENDLY INTERFEROMETRY

The previous section emphasized that the Fourier transform method of carrier fringe analysis is a powerful tool for dynamic environments, and is even more capable when complimented with PSI techniques. This combination is called environmentally friendly interferometry (EFI). In what follows I will provide examples of this synergy. Fourier transform fringe analysis has been implemented in our instruments with an analysis procedure called FlashPhase[19] and follows the methodology described in the preceding section. The apparatus used in this paper is a typical PSI interferometer shown in Figure 1 and consists of a Fizeau interferometer geometry with 5 main components, a laser, high quality reference surface, phase shifter (typically a piezoelectric transducer (PZT)), camera, and computer. For convenience the interferometer setup is shown for the measurement of flat surfaces, but the following discussion is also valid for the measurement of spherical surfaces. Throughout this paper I refer to a single camera frame of data as a spatial interferogram and the time-varying pattern of intensities observed by a pixel from a sequence of phase-shifted frames as a temporal interferogram. Thus there are as many unique temporal interferograms as there are pixels, and each has a length that equals the number of spatial interferograms acquired.

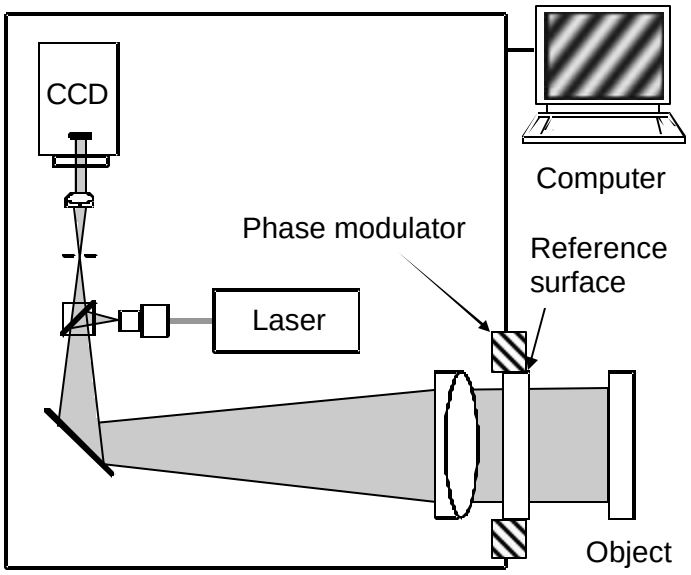

Figure 1: Basic Fizeau wave-front measuring interferometer showing the five main components

3.1. Filter considerations

As mentioned before, the lateral resolution of the method depends significantly on the characteristics of the filter used to isolate the carrier signal. The typical filter consists of a function which smoothly transitions to zero at a defined distance from the identified carrier frequency, for example the Gaussian

$$G(\vec{k}) = \exp\left[-\left(\vec{k}-\vec{k}_0\right)^2 \Big/ 2\sigma^2\right], \tag{6}$$

works well with σ defining the filter width. Since the filter width must be narrow enough to exclude DC and harmonics of the carrier frequency, this filter choice can significantly restrict the measurement lateral resolution. Therefore we employ a partially exclusive filter defined by three parameters, the width of the inclusive filter about the carrier frequency, the width of an exclusive filter about the carrier 2nd harmonic, and the width of an exclusive filter about DC. By using only the exclusive filters for example, the maximum spatial frequency content is preserved and the highest resolution obtained, albeit at the cost of preserving the noise content. Figure 2 demonstrates the lateral resolution improvement realized with the exclusive filter, which provides a lateral resolution very dose to the ½ Nyquist limit.

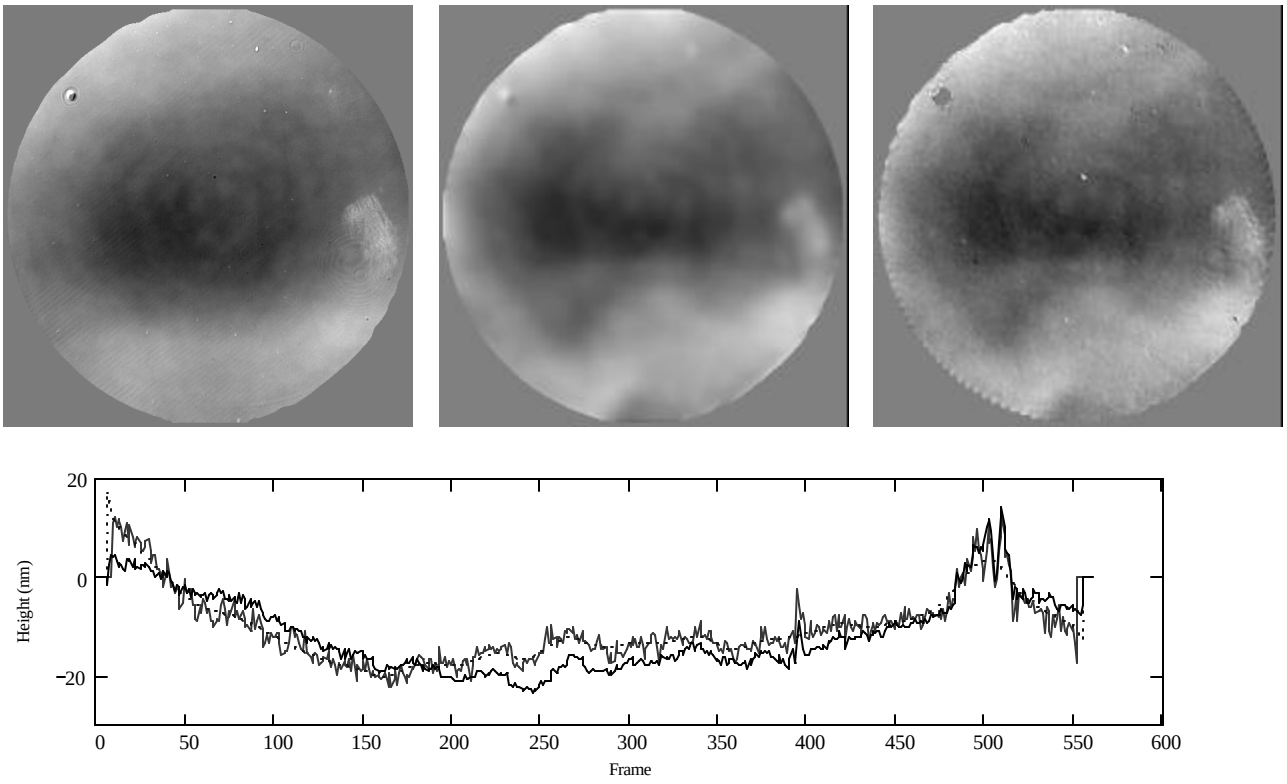

Figure 2: Comparison of the profiles measured with PSI (upper left), FlashPhase using a Gaussian inclusive filter (center) and using just the exclusive filters (upper right). Line profiles across the center are shown below, FlashPhase with the exclusive filter (thin gray) retains the high spatial frequency structure in good agreement with the PSI trace (thick black), but with a higher noise level, while the Gaussian filter result (dotted) exhibits significant rounding.

3.2. Aberration subtraction

The enhanced processing capability of modern computers allows the removal of aberrations caused by the tilted geometry to a high degree of accuracy. Two methods for performing this function were described in Section 2. The efficacy of the 1st method, subtracting a tilt dependent aberration map calculated from a raytrace simulation of the system optical prescription, is demonstrated in Figure 3. The Figure shows the results of measuring a 25mm radius spherical surface with an f/1.0 transmission sphere using PSI and FlashPhase with and without subtracting the aberration map. The peak-valley deviation between the PSI surface and the subtracted FlashPhase surface was within 6nm.

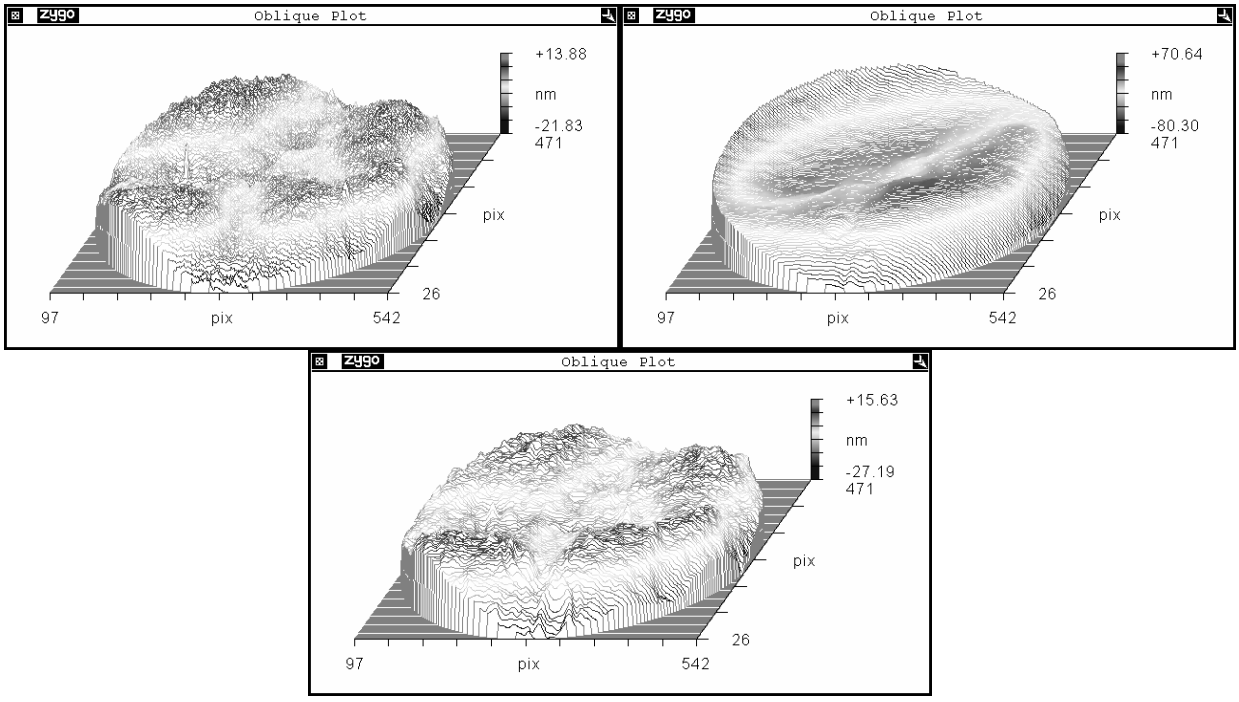

Figure 3: This series of figures shows the measurement of a 25mm radius sphere with an F1.0 transmission sphere using a standard PSI measurement with nulled fringes (top left), a Carrier fringe measurement with 50 fringes across the field (top right) and the carrier fringe result after subtraction of a tilt dependent, raytrace generated aberration map (bottom). The peak-valley deviation between the left and right profiles was less than 6nm.

3.3. Edge artifact reduction

The relative size and appearance of the Gibbs phenomenon edge artifacts depends on fringe density. As the fringe density decreases, the artifacts increase in size and amplitude. Figure 4 shows typical artifacts obtained for a fringe density of about 30 fringes across the aperture. The accompanying trace shows the profile across the diagonal. The magnitude of the edge oscillation for 30 fringes across the field is between 20-40nm peak-valley and is confined to within 5 pixels of the surface edge. There is also a strong correlation with the fringe direction.

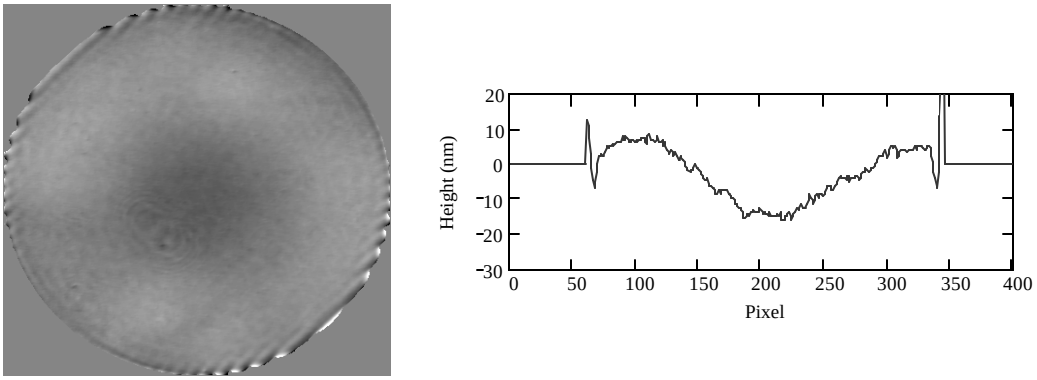

Figure 4: FlashPhase measurement of a flat with 30 fringes – note edge artifacts

Assuming the pixels cannot simply be trimmed away, there are at least three ways to deal with this phenomenon. First, is to perform additional processing referred to as analytic continuation, which involves extending the fringe periodicity into the non-surface region and smoothly transitioning to zero to the edges if the field. The second approach involves averaging N frames with $2\pi/N$ radians of phase shift between them (N = 2). Since the phase of the artifact ripple follows the fringe phase, the distortion averages out. Figure 5 shows the results of this procedure with an average of four 90-degree phase shifts, the residual ripple is reduced to be less than 1nm (see accompanying diagonal trace). Note that this technique does not depend on surface shape and thus is easy to implement. Averging provides the added bonus of noise reduction. The last approach is a combined spatial and temporal processing technique, discussed in the next section in more detail.

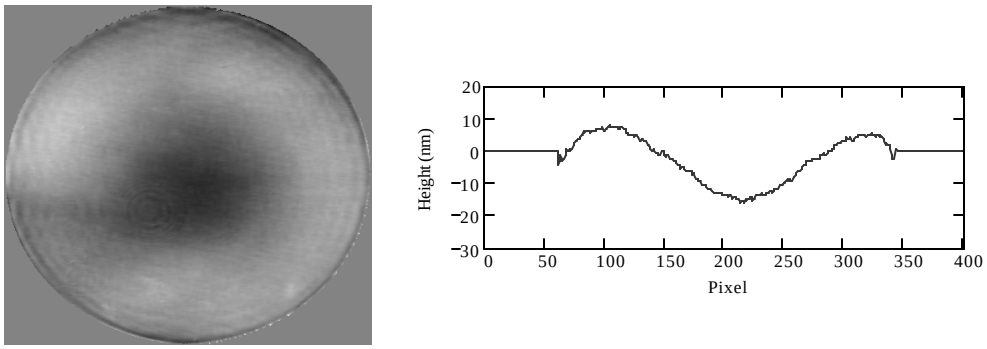

Figure 5: FlashPhase measurement of a flat with 30 fringes, averaging four 90-degree phase shifts.

4. COMBINED PSI AND CARRIER FRINGE ANALYSIS

In this section I demonstrate how to combine both spatial and temporal processing to obtain the best features of both methods with a method similar to Goldberg[16]. A sequence of N phase shifted spatial interferograms with carrier fringes is acquired and following Eq. (5), the spatial phase of every spatial interferogram in the sequence is evaluated from the complex surface map. Though in general environmental changes or surface departure could alter the fringe spatial frequency enough to require a unique filter for each interferogram, in practice a single filter is usually adequate. In fact under most circumstances the filter can be very "strong" so that only a few spatial frequencies in the neighborhood of the 1st order frequency need be calculated. The major consideration when determining the filter strength for EFI is to assure that enough spatial frequencies are retained to adequately describe the spatial frequency content of the atmospheric turbulence – not the spatial variation of the surface structure. The stronger the filter, the fewer spatial frequencies need to be calculated and the faster the algorithm. The phase increments relative to the start of the data set j_i are then found with

$$j_i = f_i - f_0 . \tag{7}$$

where $i = 0 \ldots N-1$ and the f_i are the phases found via Eq. (5). The measured phase increments are now fed to a generalized N-sample PSI analysis that calculates the starting phase of each pixel using the temporal interferogram for that pixel. At least three samples are required to satisfy the number of unknowns, but typically more are taken. Assuming the interference is well described by a pure cosine function, the intensity of the i^{th} sample in the temporal interferogram is given by

$$I_i = a + b\cos(q + j_i) = a + B\cos(j_i) - C\sin(j_i), \tag{8}$$

where $i = 0 \ldots N-1$, j_i denotes the phase shift for sample i and with

$$B = b\cos(q) \text{ and } C = b\sin(q) . \tag{9}$$

This system of linear equations can be written in matrix notation as

$$A \cdot P = I \,, \tag{10}$$

with

$$A = \begin{bmatrix} 1 & \cos(j_0) & \sin(j_0) \\ 1 & \cos(j_1) & \sin(j_1) \\ 1 & \cos(j_2) & \sin(j_2) \\ & \vdots & \end{bmatrix}, \quad P = \begin{bmatrix} a \\ B \\ C \end{bmatrix}, \quad I = \begin{bmatrix} I_0 \\ I_1 \\ I_2 \\ \vdots \end{bmatrix}. \tag{11}$$

If Eq. (10) can be solved then the starting phase q is found with

$$q = \tan^{-1}(C/B). \tag{12}$$

Note that there is no restriction on j_i, they can be of any size, change from pixel to pixel or even be wrapped modulo 2π.

The solution of Eq. (10) is readily found using a well known procedure in linear algebra called Singular Value Decomposition (SVD). The A matrix will have N rows and m columns (with $N > m$) of real numbers, and SVD states such a matrix can ***always*** be decomposed into the product of three orthonormal matrices,

$$A = USV^T \,. \tag{13}$$

The S matrix is an $N \times m$ diagonal matrix of singular values (the square root of the eigenvalues) arranged in descending order, and U and V are matrices of eigenvectors. There is a geometric interpretation of these matrices nicely discussed in a web page by Todd Will of the University of Wisconsin - La Crosse[20], but for the current discussion, the important point is that using the properties of orthonormal matrices, A is invertible via;

$$A^{-1} = VS^{-1}U^T \,. \tag{14}$$

so the coefficient matrix P is found using

$$P = VS^{-1}U^T I \,, \tag{15}$$

and the starting phase with Eq. (12). It turns out that for over-determined systems like this, the solution provided by SVD is the least squares solution.

An important point is that in large aperture interferometry, atmospheric turbulence is always present – even in the first frame, so solving for the starting phase will include distortions due to whatever index variations happened to exist at the beginning of the acquisition. What is really desired is the ensemble average of all possible starting phases in the acquisition, which can be found by averaging the phase maps obtained by sequentially assuming each frame in the acquisition as the first frame. There is a very convenient way to do this. Since the SVD provides a least squares solution, the order of the frames after the first is unimportant. This means that the solution found with frame i as the first frame, q_i, is

$$q_i = q_0 + j_i \,, \tag{16}$$

and the ensemble average is given by

$$\overline{q} = \frac{1}{N}\sum_{i=0}^{N-1} q_i = q_0 + \frac{1}{N}\sum_{i=1}^{N-1} j_i \,. \tag{17}$$

where I have explicitly assumed $j_0 = 0$. Therefore only one starting phase needs to be solved for with SVD. The method is outlined in Figure 6.

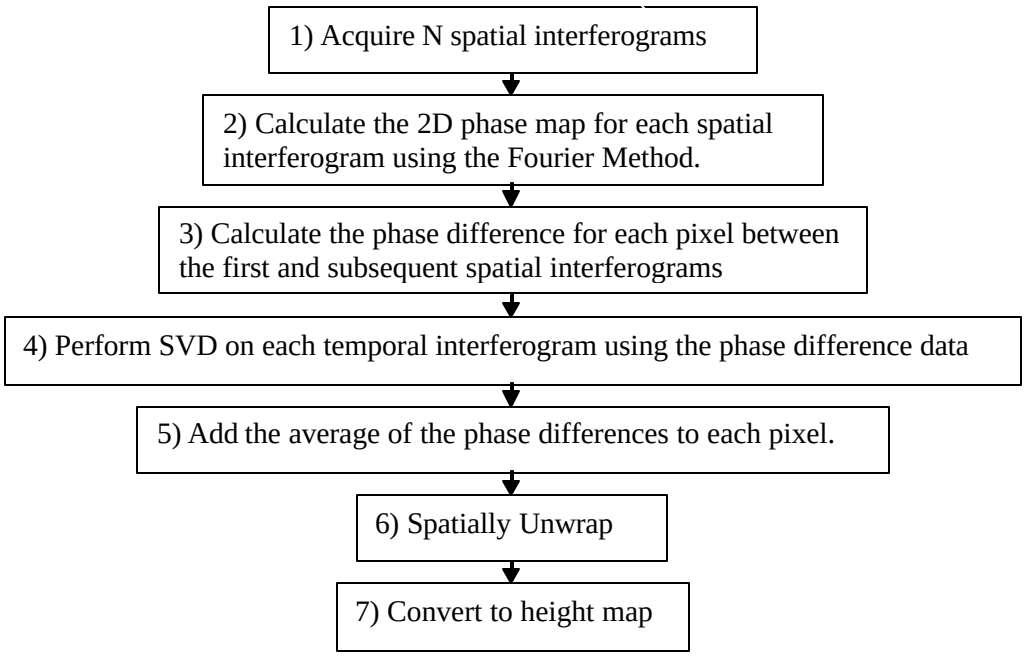

Figure 6: Flowchart outlining the method for Combining PSI with carrier fringe analysis

The only practical limitation to this method is that the sampling integration period be much shorter than the typical vibrational period so the vibrationally induced motion is frozen in each spatial interferogram with minimal fringe contrast loss. The method works exceptionally well even in environments for which traditional methods completely fail.

4.1. Example

I illustrate the method with a comparison of the measured profile of an optical flat taken under two different environmental conditions – a quiescent environment and a turbulent one. The quiescent environment consisted of a short (30mm) shielded cavity with passive isolation. The turbulent environment consisted of a long (400mm) cavity open to the air, with a PZT attached to one corner of the test object. The PZT was sinusoidally modulated with a 25nm amplitude at a frequency of 16 Hz, slightly more than half the camera frame rate of 30Hz. A sequence of 77 phase shifted spatial interferograms with approximately 30 fringes across the surface was taken in both environments and then analyzed in two ways; 1) a standard PSI analysis consisting of an average of 11 consecutive measurements using a 7-frame phase shifting algorithm[21] that expects a nominally 90^O phase increment and 2) as one data set consisting of 77 spatial interferograms using combined PSI and spatial carrier techniques.

This particular vibration frequency and amplitude was chosen to produce significant phase error using standard PSI algorithms but the frequency-amplitude product is small enough so that little fringe contrast reduction occurred during one camera integration period. A higher vibrational frequency-amplitude product could be tolerated if the camera were shutterable and a shorter integration time used. Figure 7 compares the results from the two processing methods on these two data sets. The results showed that the combined analysis in the turbulent environment produces the same surface profile (within 0.65nm rms) as PSI under quiescent conditions.

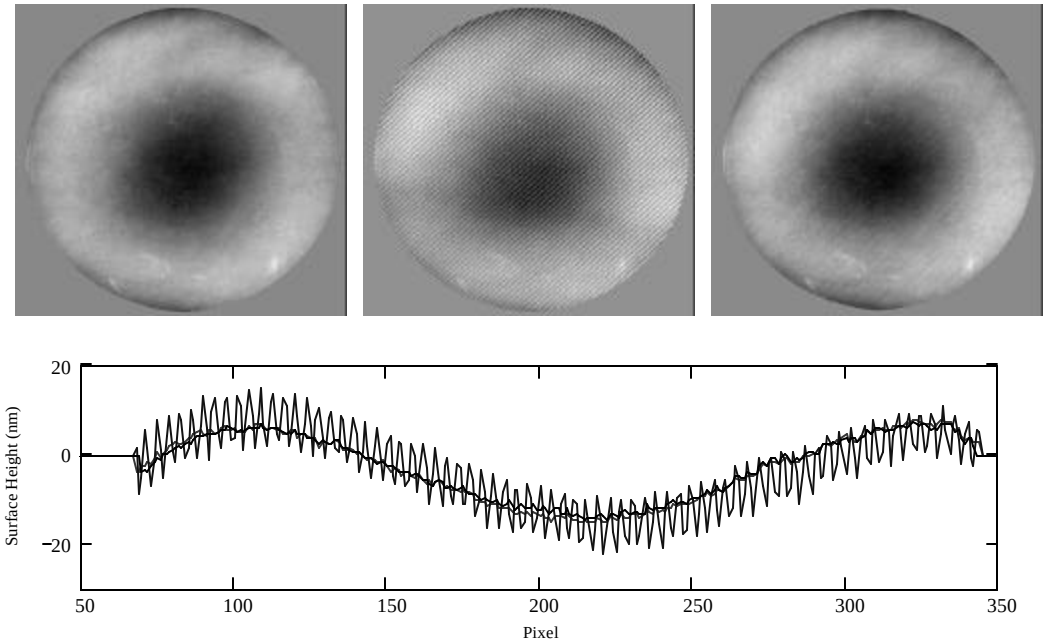

Figure 7: Comparison of traditional PSI and the combined analysis in both turbulent and quiescent conditions. The top left surface is a PSI measurement on the quiescent data and serves as a good measurement of the surface. The top middle figure is a PSI measurement under turbulent conditions and the top right figure is the surface measured using the combined analysis on the turbulent data set. Phase error is observed when analyzing the turbulent set with PSI but no significant phase error occurs with combined analysis. The rms difference between the 2D profiles measured with PSI under quiet conditions and with the combined analysis under turbulent conditions is only 0.65nm. The bottom trace represents a diagonal profile through the center of the surface perpendicular to the fringe pattern for all three profiles. Identical profiles are observed between quiescent PSI (grey) and turbulent combined analysis (black). The turbulent PSI trace (thin black) exhibits ripple at twice the fringe frequency typical for vibration with 10nm amplitude.

5. SUMMARY

Combining both PSI and spatial phase processing capability in a single instrument provides an effective high precision wave-front measuring tool for both dynamic and static environments. The combination achieves great flexibility in both environments, is self calibrating and combined with modern digital imagers and computer platforms is fast, accurate and easy to use, removing most of the historical weaknesses of spatial phase processing methods.

ACKNOWLEDGMENTS

The author gratefully acknowledges the contributions of Dan Sykora, Peter de Groot and Xavier Colonna de Lega to this work.

REFERENCES

[1] J. E. Greivenkamp and J. H. Bruning, “Phase Shifting Interferometry,” Chap. 14, of “Optical Shop Testing”, 2nd Ed., J. Wiley pub, edited by D. Malacara.

[2] J. Greivenkamp, “Generalized data reduction for heterodyne interferometry,” Opt. Eng. 23, 350-352 (1984)

[3] K. Okada, A. Sato, J. Tsujiuchi,” Simultaneous calculation of phase distribution and scanning phase shift in phase shifting interferometry,” Opt. Comm. 84, 118-124 (1991)

[4] I. Kong and S. Kim, “General algorithm of phase-shifting interferometry by iterative least-square fitting,” Opt. Eng. 34, 183-188 (1995)

[5] S. Kim, M. Kang, G. Han "Accelerated phase-measuring algorithm of least-squares for phase-shifting interferometry," Opt. Eng. 36, 3101-3106 (1997)

[6] P. L. Wizinowich, "Phase shifting interferometry in the presence of vibration: a new algorithm and system," Appl. Opt. 29(22), 3271-3279, 1990

[7] L. Deck and P. de Groot, "Punctuated quadrature phase-shifting interferometry," Opt. Lett. 23, 19-21 (1998)

[8] L. Deck, "Vibration-resistant phase-shifting interferometry," Appl. Opt. 35(34), 6655-6662 (1996)

[9] U. S. Patent # 6,304,330 to Millerd et. al.

[10] R. Smythe and R. Moore, "Instantaneous phase measuring interferometry," Opt. Eng. 23, 361 (1984)

[11] M. Takeda, I. Hideki, S. Kobayashi, "Fourier-Transform Method of Fringe-Pattern Analysis for Computer Based Topography and Interferometry," J. Opt. Soc. Am. 72, 156-160 (1982)

[12] W. Macy, "Two Dimensional Fringe Pattern Analysis," Appl. Opt. 22, 3898-3901 (1983)

[13] D. Malacara and S. DeVore, "Interferogram Evaluation and Wavefront Fitting", Chap. 13, of "Optical Shop Testing", 2nd Ed., J. Wiley pub, edited by D. Malacara.

[14] M. Küchel, "The new Zeiss Interferometer," Proc. SPIE, 1332, 655-663 (1990)

[15] U.S. Pat. No. 5,343,294 to Küchel and Hof

[16] K.A. Goldberg and J. Bokor, "Fourier-transform method of phase-shift determination," Appl. Opt. 40(17), 2886-2894 (2001)

[17] C.J. Evans, "Compensation for errors introduced by non-zero fringe densities in phase measuring interferometers," CIRP Annals, 42(1), 577-580 (1993)

[18] R.W. Gerchberg. "Super-resolution through error energy reduction," Opt. Acta 21, 709 (1974)

[19] FlashPhase™ is a registered trademark name for the Fourier transform technique incorporated in Zygo interferometers

[20] See http://www.uwlax.edu/faculty/will/svd/index.html

[21] P. de Groot, "Derivation of algorithms for phase-shifting interferometry using the concept of a data-sampling window," Appl. Opt. 34(22), 4723-4730 (1995)